ACS APPLIED MATERIALS & INTERFACES

www.acsami.org

Research Article

Hierarchically Ordered Silicon Metastructures from Improved Self-Assembly-Based Nanosphere Lithography

Xiaoguo Fang, Changxiong Zheng, Zhen Yin, Zhenming Wang, Jiawei Wang, Jianxun Liu, Dan Luo, and Yan Jun Liu*

Cite This: *ACS Appl. Mater. Interfaces* 2020, 12, 12345−12352

Read Online

ACCESS | Metrics & More | Article Recommendations | Supporting Information

ABSTRACT: We developed an improved self-assembly method to obtain a large-area, high-quality templated monolayer mask using the polystyrene spheres. On the basis of the templated mask, hierarchically ordered Si metastructures with different nanosteps are fabricated using cyclic inductively coupled plasma etching technique. By evaporating a thin gold capping layer on these Si metastructures, their optical properties are comparatively studied using the surface-enhanced Raman scattering spectroscopy. Our proposed technique is highly promising for fabricating a variety of periodic three-dimensional hierarchically ordered metastructures, which could be further utilized for applications in SERS-based biosensors, optical absorbers, metamaterial/metasurface devices, etc.

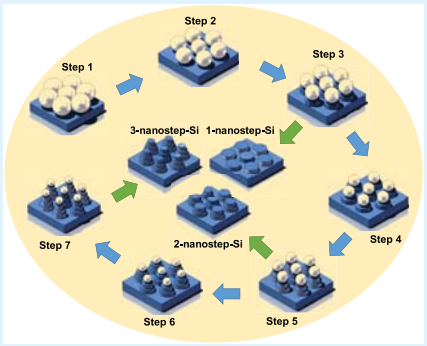

KEYWORDS: *self-assembly, 3D lithography, nanosphere lithography, hierarchical metastructure, plasmonic enhancement*

INTRODUCTION

Ultracompact, cost-effective, and integrable analytical devices with unprecedented performance present an ever-increasing need in various application fields, such as life care, environmental monitoring, food safety, and defense. Advances in micro/nanofabrication technologies could make it possible to replace the conventional bulky components.[1−3] For instance, a variety of silicon nanostructures, such as pyramids, holes, wires, pillars, tubes, and cones have been designed and applied in solar cells,[4,5] biosensors,[6,7] and drug delivery systems[8,9] because of their superior optical/electrical properties, biocompatibility, and mechanical properties. Because of its high refractive index and compatibility with CMOS processes, silicon has also been widely used to construct all-dielectric metasurface devices, including flat lenses,[10,11] structural colors,[12] holograms,[13] nonlinear devices,[14] etc. However, despite their attractive interest and broad applicability, the deployment of hierarchical silicon nanostructures with dimensional control has been limited by the lack of a simple and scalable fabrication technique.

Although it is still possible to achieve hierarchical silicon nanostructures using the current micro/nanofabrication techniques, such as photolithography, electron-beam lithography, and focused ion-beam milling, complicated multistep, time-consuming, and low-throughput processes are usually inevitable. Comparatively, nanosphere lithography (NSL), also known as colloidal lithography, holds great advantages because of its high throughput and low cost.[15] NSL employs a self-assembled, close-packed monolayer or bilayer of colloidal nanospheres (e.g., polystyrene, SiO_2, and others) as the templated masks to create patterns on the underneath substrates.[16] Various structures, such as disks,[16−18] circular rings,[19−22] triangles,[23] and crescents,[24] have been generated at the nanoscale using this technique. Usually, this kind of templated masks is used only once during the lithographic process. This "one-time use" approach greatly restricts the fabrication of nanostructures with precise dimensional control, hence limiting the potential of the NSL technique. Recently, Xu et al. reported the fabrication of periodic three-dimensional hierarchical silicon nanostructures using a multiple-patterning NSL combined with Bosch process, in which the monolayer nanosphere mask was used multiple times.[25] However, it involves cyclic, complex passivation and etching processes, making the whole process complicated and costly. On the other hand, multiscale hierarchical nanostructures have triggered great interests in many applications including biomedical detection,[26] mixture separation,[27] liquid-repellence,[28] and lab-on-a-chip devices.[29] Therefore, it is highly demanding to have simple fabrication processes to achieve those multiscale hierarchical nanostructures.

Received: December 19, 2019
Accepted: February 18, 2020
Published: February 18, 2020

The great potential of the NSL technique, to a large extent, is predetermined by the quality of the templated mask via the self-assembly process. We have extensively studied the self-assembly processes for opals and inverse opals in two- and three-dimensional manners with various nanosphere sizes.[30−35] In this work, we develop an improved self-assembly method to obtain a large-area, high-quality templated monolayer mask using the polystyrene (PS) spheres. With cyclic inductively coupled plasma (ICP) etching processes, hierarchically ordered Si metastructures with different nanosteps are fabricated. With a gold capping layer on these Si metastructures, their optical properties are comparatively studied using the surface-enhanced Raman scattering (SERS) spectroscopy. Our proposed technique is highly promising for fabricating a variety of periodic 3D hierarchically ordered metastructures, which could be further utilized for applications in SERS-based biosensors, optical absorbers, metamaterial/metasurface devices, etc.

MATERIALS AND METHODS

Materials. All silicon wafers with a 150 mm diameter (P-Type, < 100>) were purchased from Beijing Youran Yisen Technology Co., Ltd. (Beijing, China). Polystyrene (PS) sphere latex solution (2.5 wt % dispersion in water) was purchased from Alfa Aesar (China) Chemical Co., Ltd. (Shanghai, China). All silicon substrates used in the process were treated for 15 min with UV−O_3 cleaner (BZS250GF-TC), which was purchased from HWOTECH (Shenzhen, China).

Templated Mask on Si Substrates. The templated mask for multiple NSL consists of a monolayer of PS spheres, which was formed via an improved self-assembly method at the air−liquid interface. The self-assembly process for the PS monolayer is schematically described in Figure 1. First, a layer of deionized water

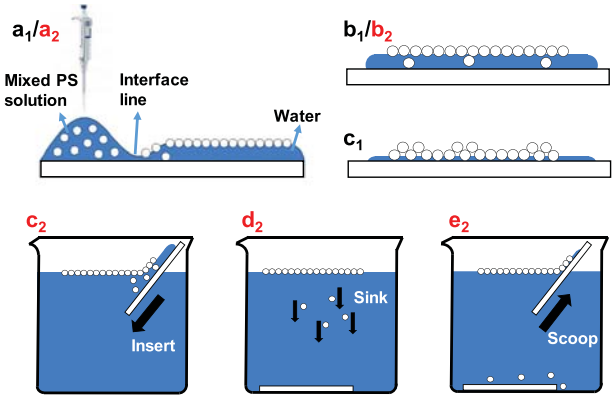

Figure 1. (a) Schematic illustration of fabricating the templated PS sphere monolayer mask on Si substrates using the (a_1−c_1) conventional and (a_2−e_2) improved air−liquid interface self-assembly methods, respectively.

(~60 μL) was spread on a clean silicon wafer (2 cm × 2 cm). A 20 μL mixed PS solution (ethanol and 2.5 wt % PS aqueous solution with a volume ratio of 1:1) was then added from a corner of the Si substrate (Figure 1a_1). Due to the strong hydrophobicity of the PS spheres, the covered water on the substrate was pushed to another side. Soon the water would be gradually recovered because the ethanol in the mixed PS solution was miscible with the water. A PS monolayer was then formed at the air−water interface (Figure 1b_1). Thus, the drip rate and the stable "interface line" between mixed PS solution and water are crucial to the quality of the monolayer formation (Figure 1a_1). After a period of natural evaporation, the PS sphere monolayer was finally deposited on the Si wafer (Figure 1c_1). This forming process is considered as the conventional self-assembly method (Figure 1a_1−c_1).

We used a slightly modified method to further improve the monolayer quality (Figure 1a_2−e_2). Before the monolayer depositing on the silicon wafer, we further inserted the Si substrate with the PS monolayer into the DI water (Figure 1c_2). With the surface tension of the water, the PS monolayer still kept floating on the surface of the water, however, those spheres that originally diffused into the water would gradually sink into the bottom (Figure 1d_2) since the PS density is larger than the water one (ρ_{PS} = 1.06 g/cm^3). With the only PS monolayer floating at the air−water interface, we used another clean, hydrophilic Si substrate to scoop this monolayer, as illustrated in Figure 1e_2. As a result, we could achieve a templated PS monolayer mask with much more improved quality.

Cyclic Etching Processes. With the templated PS monolayer mask on the Si substrate being ready, the PS spheres and the silicon underwent alternate etching by cycles of different gases via inductively coupled plasma (ICP, GSE200Plus, Northern Microelectronics) process. The cyclic etching processes of the multiple NSL are depicted in Figure 2. In our experiments, the PS spheres and the

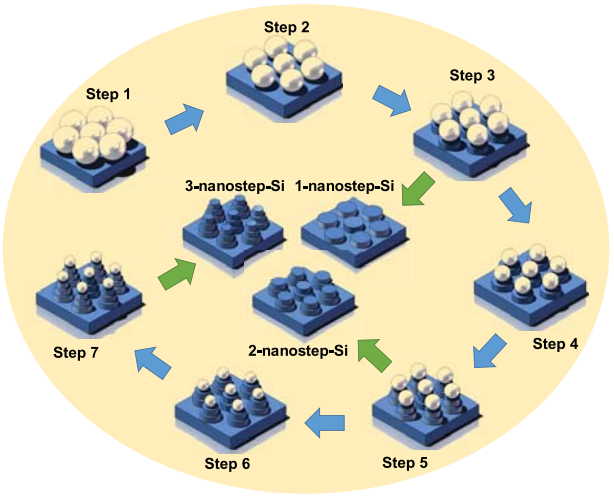

Figure 2. Schematic illustration of the fabrication processes for the nanostepped Si metastructures. Step 1: A PS monolayer is transferred to a clean silicon substrate and then dried naturally. The diameter of the PS sphere defines the period of nanostepped arrays. Step 2: The PS spheres are selectively etched for 12 s using the oxygen plasma to reduce the sphere size. The reduced sphere size determines the diameter of 1-nanostep-Si metastructures. Step 3: The silicon substrate is selectively etched for 120 s using the mixed SF_6 and CHF_3 plasma. The etching depth (height) is determined by the etching power and time. By etching the PS spheres completely using the oxygen plasma, the 1-nanostep-Si metastructures will be then achieved. Step 4: The 2nd time etching of PS spheres for 84 s further defines the diameter of the 2nd Si nanostep. Step 5: The 2nd time etching of silicon for 80 s further defines the depth of the 2nd Si nanostep. Step 6: The 3rd time etching of PS spheres for 20 s further defines the diameter of the 3rd Si nanostep. Step 7: The 3rd time etching of silicon for 70 s further defines the depth of the 3rd Si nanostep.

silicon were selectively etched by using the O_2 plasma and the mixed gas of SF_6 and HCF_3, respectively. During the PS etching step, a flow of 50 sccm O_2 was used with ICP power 100 W, bias power 20 W at a pressure of 8 mTorr. The Si substrate with PS monolayer as the mask was etched by ICP using a gas mixture of SF_6 (12 sccm) and HCF_3 (70 sccm) at 10 mTorr with ICP power 300 W and bias power 50 W. The ICP etching recipes for the PS spheres and the silicon were summarized in Table 1. From Figure 2, we can see that with each cyclic etching process, a nanostepped Si metastructure can be

https://dx.doi.org/10.1021/acsami.9b22932
ACS Appl. Mater. Interfaces 2020, 12, 12345−12352

Table 1. Respective Etching Recipes of the PS Spheres and Silicon Substrate

	Si etching	PS etching
pressure (mTorr)	10	8
gas	SF_6/CHF_3	O_2
gas flow rate (sccm)	12/70	50
SrcRF_Power (W)	300	100
BiasRF_Power (W)	50	20

achieved by removing the PS spheres. The PS spheres were completely removed by simply using the O_2 plasma with the etching time of 800 s. The diameter and depth of each nanostep were notably defined by the etching time of the oxygen plasma and the mixed SF_6 and HCF_3 plasma, respectively.

Metal Coating. Once we achieved the Si metastructures with different nanosteps, additional gold coatings were carried out by loading them into the vacuum chamber of an E-beam evaporator (TF500, British HHV). A 30 nm thick gold film was deposited on Si metastructures with 5 nm Cr thin film as the adhesion layer using electron-beam evaporation. In order to reduce the roughness and increase the adhesion of the metal film, low evaporation rates were applied (~3 and ~0.2 Å/s for gold and Cr films, respectively). Both Cr and gold films were sequentially deposited on Si metastructures without breaking the vacuum in the evaporator chamber at a base pressure of 5×10^{-6} Torr.

Characterization. The morphology, size distribution, and composition of as-prepared nanocrystals were investigated by the field-emission scanning electron microscopy (FESEM, Merlin, Zeiss). The surface-enhanced Raman scattering (SERS) spectra were collected with a confocal Raman system (Ahpha300, WITec). We used an objective lens (50×, NA = 0.5) to focus the excitation laser light (working wavelength: 532 nm) onto the samples and collect the Raman signal to the spectrometer. A Rhodamine 6G (R6G) solution with different concentrations from 1×10^{-2} to 1×10^{-6} M were used to evaluate the SERS performance of the prepared metastructures. A 2 μL R6G solution was dropped onto different samples and the droplets were dried in the air at room temperature for 30 min. To ensure the repeatability, we averaged the spectra by taking multiple measurements at different positions. Each spectrum was taken with the integration time of 10 s.

RESULTS AND DISCUSSION

For the NSL technique, the templated PS monolayer mask plays a key role. As such, the formation of a large-area, high-quality self-assembled monolayer is a prerequisite. Given that the self-assembly is a deliberately controlled process, it is usually challenging to achieve the large-area, high-quality self-assembled monolayer. As illustrated in Figure 1a$_1$–c$_1$, in the conventional self-assembly process, although most PS spheres will form a floating monolayer at the air–water interface, a small amount of PS spheres will also diffuse into the water. As the water evaporates, those diffused spheres inside the water will lift up three spheres in the monolayer, creating many observable "triple" defects, as shown in Figure 3a. A further close look confirms this lift-up issue, as highlighted in Figure 3b. The observed "triple" defects affect severely the quality of the templated mask and the fabricated metastructures subsequently. Although the number of the "triple" defects can be further minimized by the deliberate control of the self-assembly conditions, it will greatly increase the complexity and fabrication cost.

In order to achieve a high-quality self-assembled monolayer, we used a slightly modified method to further decrease the number of this kind of defect (Figure 1a$_2$–1e$_2$). We used another silicon substrate to salvage the monolayer at the air–water interface by giving up those spheres sinking into the bottom. With these additional and simple steps, the "triple" defects can be completely eliminated. Hence we could achieve a large-area, high-quality, defect-free templated mask. Figure 3c, d shows the achieved monolayer of PS spheres. The key processes are also illustrated by the short videos (see Videos S1–S3). It is worth mentioning that after the PS monolayer is formed on the Si substrate, as shown in Figure 1b$_2$, there exist numerous liquid bridges (i.e., the liquid gaps) between the PS sphere. As the monolayer is still floating on the liquid–air interface, a wetting-caused capillary force will be formed in these liquid bridges.[36] This capillary force will keep the PS monolayer in a metastable state. With delicate and careful handling, when the PS monolayer is transferred on the surface of water by inserting the Si substrate (Figure 1c$_2$) or scooping

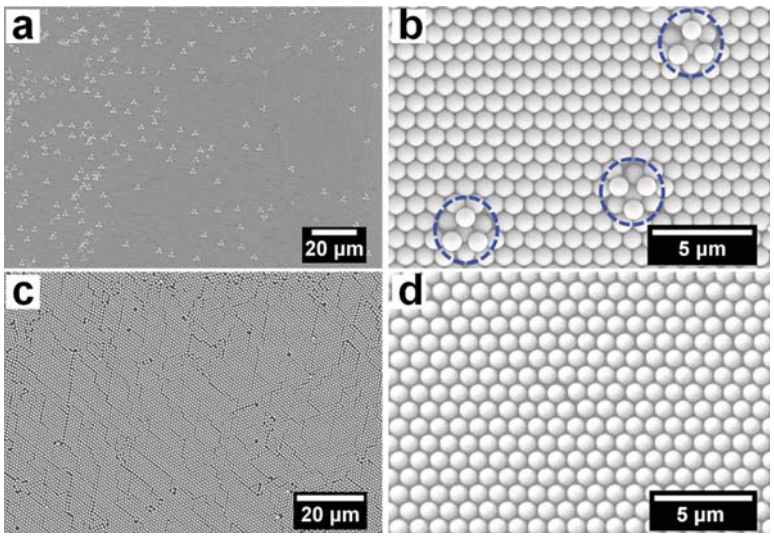

Figure 3. (a, c) Large-area and (b, d) magnified SEM images of templated PS sphere monolayer by conventional and our modified self-assembly methods, respectively.

https://dx.doi.org/10.1021/acsami.9b22932
ACS Appl. Mater. Interfaces 2020, 12, 12345–12352

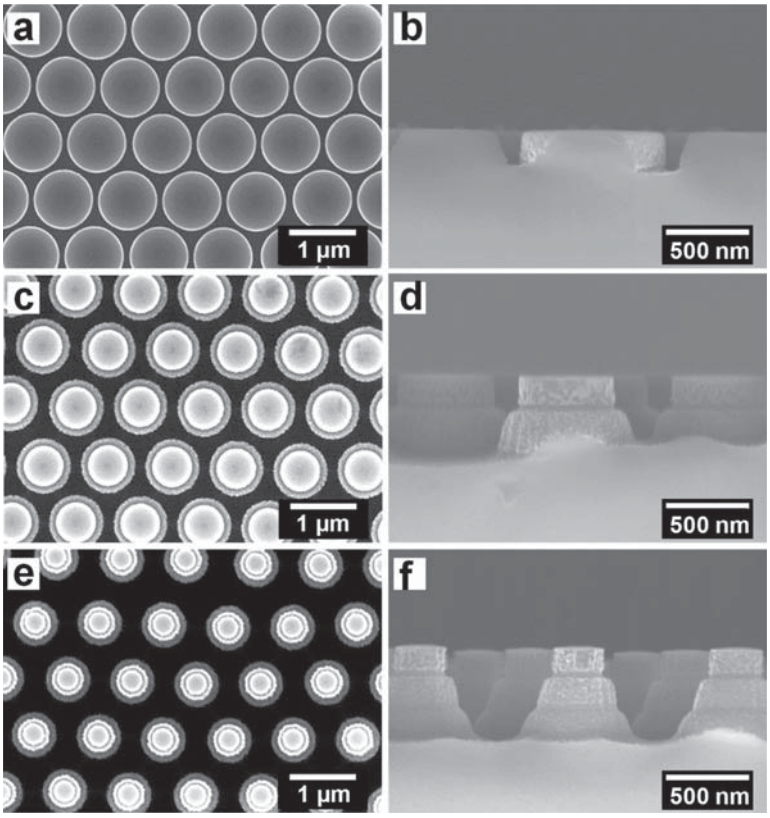

Figure 4. Si metastructures with different nanosteps fabricated by multiple NSL technique: (a, c, and e) top-view and (b, d, and f) side-view SEM images of metastructures with one, two, and three nanosteps.

the PS monolayer (Figure 1e_2), we can therefore see that the PS monolayer still keeps in its original form without any damages, as shown in Videos S2 and S3. In addition, after the PS monolayer was scooped with another Si substrate, the drying process does not affect the monolayer quality significantly. This can be confirmed from the experimental results (Figure 3c, d). From Figure 1, we add three additional steps (Figure 1c_2−e_2) with the purpose of eliminating the "triple" defects. These additional steps might increase the possibility of creating more "streak" defects, which typically exist in all kinds of self-assembly techniques. Overall, we improve the monolayer quality in a large area, which is particularly beneficial to the NSL process because the "triple" defects will cause much more observable defects compared to the "streak" defects during the lithographic process. Compared to the conventional self-assembly method, it clearly shows that our modified approach provides much better quality of the PS monolayer. In our experiments, we used PS spheres with a diameter of 1 μm to fabricate the templated monolayer mask, which gives the the mask a period of 1 μm as well.

With the achieved large-area, high-quality templated mask, we can then use it for multiple NSL, which is a "true 3D fabrication technique" compared to traditional one-time NSL. As shown in Figure 2, the initial size of PS spheres is used to control the period, whereas the etching time of the oxygen plasma and the mixed SF_6 and CHF_3 plasma is used to regulate the radius and depth of the nanosteps, respectively. However, it is worth mentioning that in fact, during the silicon etching process by using the mixed SF_6 and CHF_3 plasma, the silicon nanosteps were etched both vertically and laterally, which makes it a great challenge to achieve multiple nanosteps. In our experiments, we managed to achieve multistepped Si metastructures, as shown in Figure 4. We can clearly see that with the simple cyclic ICP processes, one-, two-, and three-nanostepped hierarchical Si metastructures are fabricated. A further close look at the magnified images shows that only the first nanostep from the top shows a vertical sidewall, whereas the second and subsequent ones show slightly sloped sidewalls. We noticed that hierarchically ordered Si nanostructures have also been reported by Xu and co-workers.[25] Compare to our approach, their technique is much more complicated and costly because cyclic and complex passivation and etching processes are involved. In addition, in their work, in order to achieve the vertical sidewall, they used the Bosch process, which makes the sidewalls have many "ripples" with about 25 nm roughness. Comparatively, our cyclic ICP processes make the sidewall much smoother. The sloped and smooth sidewall of the nanosteps will also facilitate the uniform and conformal coatings of other materials on the fabricated Si metastructures.

As an example, we have deposited a thin layer of gold film onto the achieved Si metastructures. Figure 5 shows the SEM images of nanosteps after evaporating a 30 nm thick gold film. We can clearly observe that the silicon stepped structures were nearly conformally covered by the thin deposited gold layer, which guarantees the excellent uniformity of these hierarchically ordered silicon metastructures. We foresee that such plasmonic-material-capped (e.g., gold, silver, aluminum) Si metastructures could present intriguing possibilities to design and engineer the optical properties, which could be of great

https://dx.doi.org/10.1021/acsami.9b22932
ACS Appl. Mater. Interfaces 2020, 12, 12345−12352

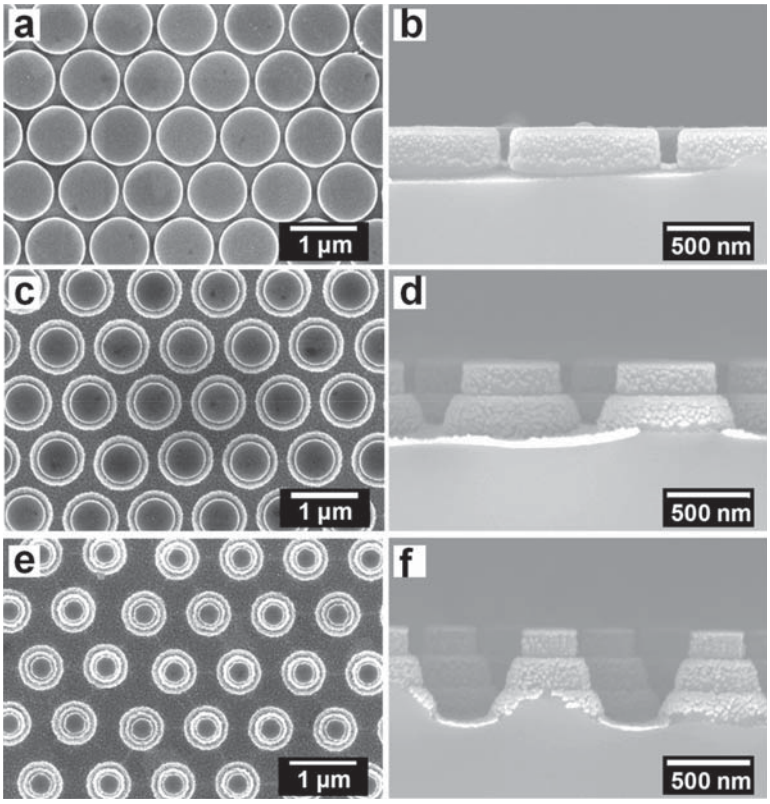

Figure 5. Thirty-nanometer-thick gold-capped Si metastructures with different nanosteps: (a, c, and e) top-view and (b, d, and f) side-view SEM images of metastructures with one, two, and three nanosteps.

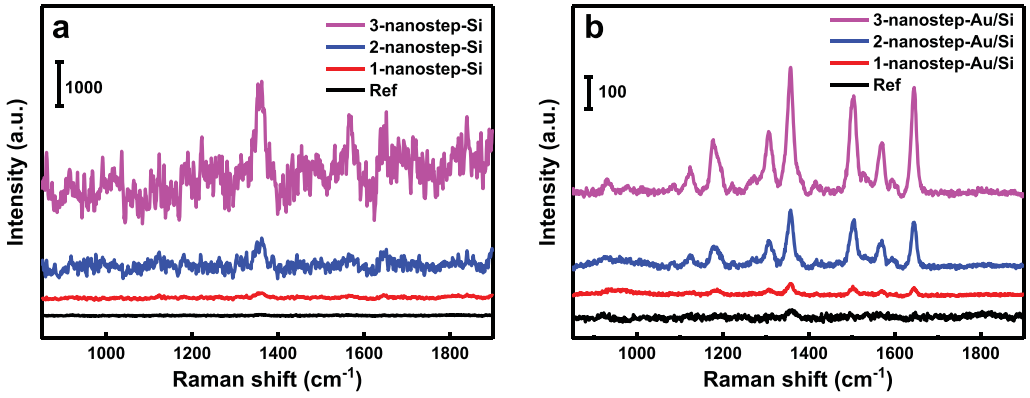

Figure 6. SERS spectra for R6G with the concentration of 1×10^{-3} M and 1×10^{-6} M on the (a) pure Si and (b) gold-capped Si metastructures with different nanosteps. The SERS spectra were achieved under 532 nm laser excitation power of 180 $\mu W/\mu m^2$ for the pure Si metastructures and 160 $\mu W/\mu m^2$ for the gold-capped Si metastructures with the same integration time of 10 s. The black references in both a and b correspond to SERS spectra of R6G (10^{-2} M) obtained on the silicon wafer under 532 nm laser excitation at 80 $\mu W/\mu m^2$ with an integration time of 10 s.

importance for potential applications in biosensing and surface-enhanced spectroscopies.

These hierarchically ordered 3D Si metastructures provide numerous gaps both laterally and vertically, which could localize electromagnetic fields strongly. With gold layer capping, the gold nanostructures themselves possess strong localized surface plasmon resonances (LSPRs); moreover, strong plasmonic coupling also occurs between the neighboring nanostructures. Hence, there are a great number of hot spots generated in these hierarchically ordered 3D Si metastructures upon light excitation, which can enhance the localized electromagnetic fields directly.[37−41] Therefore, we used the SERS technique to characterize how strong the hierarchically ordered 3D Si metastructures localize the electromagnetic fields. Figure 6a, b shows a series of comparative SERS spectra for R6G with the concentration of 1×10^{-3} M and 1×10^{-6} M on the pure Si and gold-capped Si metastructures with different nanosteps, respectively. The peak positions and relative amplitudes of these spectra for R6G molecules are consistent with previous results.[42] It is obvious that with the gold-capping layer, the SERS signals are significantly enhanced, which can be attributed to the

https://dx.doi.org/10.1021/acsami.9b22932
ACS Appl. Mater. Interfaces 2020, 12, 12345−12352

plasmon-enhanced localization of the electromagnetic fields. To quantify the enhancement contribution from these hierarchically ordered 3D Si metastructures, we calculated the enhancement factor (EF) based on the following formula

$$\mathrm{EF} = \frac{I_{\mathrm{SERS}}/C_{\mathrm{SERS}}}{I_{\mathrm{NR}}/C_{\mathrm{NR}}} \quad (1)$$

where I_{SERS} is the SERS intensity of the R6G characteristic peak of 1358 cm^{-1}, I_{NR} denotes the normal Raman scattering intensity of the same peak. C_{SERS} and C_{NR} are the concentrations of R6G solutions that were applied onto the samples. From Figure 6a, we can calculate the EFs for R6G SERS signals on the pure Si metastructures, $\mathrm{EF}_{\text{1-nanostep-Si}} = 1.56 \times 10$, $\mathrm{EF}_{\text{2-nanostep-Si}} = 1.00 \times 10^2$, $\mathrm{EF}_{\text{3-nanostep-Si}} = 3.35 \times 10^2$. Similarly, from Figure 6b, we can also obtain the EFs for R6G SERS on the gold-capped Si metastructures, $\mathrm{EF}_{\text{1-nanostep-Au/Si}} = 5.37 \times 10^3$, $\mathrm{EF}_{\text{2-nanostep-Au/Si}} = 2.65 \times 10^4$, $\mathrm{EF}_{\text{3-nanostep-Au/Si}} = 5.67 \times 10^4$. We can therefore see that, for both pure and gold-capped Si metastructures, the greater the number of the nanosteps, the stronger the enhanced SERS signals. More importantly, the gold-capped Si metastructures demonstrate enhanced SERS signals two orders of magnitude greater than the pure Si ones with the same number nanosteps. For the gold-capped Si metastructures, those with two and three nanosteps have the same level of enhancement, whereas those with one nanostep have obviously much weaker enhancement. This observation indicates that the slopes play a particularly important role for the formation of more hot spots that subsequently enhance the SERS signals. It is worth mentioning that both the pure and gold-capped Si metastructures have not been optimized for SERS signal detection in this work. We believe with purposed designs (e.g., further decreasing the period of the metastructures), the SERS signals could be further significantly enhanced and the detection of limit can then be further decreased as well.

CONCLUSIONS

In summary, we have demonstrated a facile and large area fabrication of hierarchically ordered Si metastructures based on an improved self-assembly NSL. This fabrication technique features two important advantageous points: (1) With just simple additional steps, a large area and much more uniform self-assembled PS monolayer can be achieved, which plays a key role for subsequent lithography process; (2) The simple multicycle etching processes provides a well-defined nano-stepped silicon structures with slight slopes, which favors a uniform and conformal coating for other materials, especially the plasmonic materials. In addition, our proposed approach is not limited to the Si material. As long as the selected base material has a well-differentiated etching ratio with the PS monolayer mask, it will be easy to obtain the multilayered metastructure of the base materials. This lithographic technique is compatible with and could be integrated into other micro/nanoscale device manufacturing (for instance, microfluidic technology) to add additional functions through rational 3D designs. The achieved results suggest that our fabrication technique is a highly promising 3D nanolithographic technique to achieve a variety of periodic 3D hierarchically ordered metastructures, which could find many potential applications in SERS-based biosensors, optical absorbers, metamaterial/metasurface devices, etc.

ASSOCIATED CONTENT

Supporting Information

The Supporting Information is available free of charge at https://pubs.acs.org/doi/10.1021/acsami.9b22932.

Video S1: Demonstration video of PS nanospheres self-assembly process corresponding to Figure $1a_1/a_2$. The video has been accelerated 10 times (MP4)

Video S2: Demonstration video of inserting Si substrate with PS monolayer into water corresponding to Figure $1c_2$. The video has been accelerated 2 times. In this process, it is important to reduce the effects of airflow (MP4)

Video S3: Demonstration video of scooping the PS monolayer process corresponding to Figure $1e_2$. The video has been accelerated 2 times. In addition, it can also be used to transfer the monolayer to any hydrophilic substrate, even with a curved surface (MP4)

AUTHOR INFORMATION

Corresponding Author

Yan Jun Liu − *Department of Electrical and Electronic Engineering, Southern University of Science and Technology, Shenzhen 518055, China;* orcid.org/0000-0001-8724-0434; Email: yjliu@sustech.edu.cn

Authors

Xiaoguo Fang − *Department of Electrical and Electronic Engineering, Southern University of Science and Technology, Shenzhen 518055, China; Harbin Institute of Technology, Harbin 150001, China*

Changxiong Zheng − *Department of Electrical and Electronic Engineering, Southern University of Science and Technology, Shenzhen 518055, China*

Zhen Yin − *Department of Electrical and Electronic Engineering, Southern University of Science and Technology, Shenzhen 518055, China*

Zhenming Wang − *Department of Electrical and Electronic Engineering, Southern University of Science and Technology, Shenzhen 518055, China*

Jiawei Wang − *Department of Electrical and Electronic Engineering, Southern University of Science and Technology, Shenzhen 518055, China*

Jianxun Liu − *Department of Electrical and Electronic Engineering, Southern University of Science and Technology, Shenzhen 518055, China*

Dan Luo − *Department of Electrical and Electronic Engineering, Southern University of Science and Technology, Shenzhen 518055, China;* orcid.org/0000-0003-2117-0570

Complete contact information is available at: https://pubs.acs.org/10.1021/acsami.9b22932

Notes

The authors declare no competing financial interest.

ACKNOWLEDGMENTS

This work was supported in part by National Natural Science Foundation of China (Grant 61805113), Guangdong Innovative and Entrepreneurial Research Team Program (Grant 2017ZT07C071), Natural Science Foundation of Guangdong Province (Grants 2017A030313034 and 2018A030310224), and Shenzhen Science and Technology

Innovation Commission (Grants JCYJ20170817111349280, JCYJ20180305180635082, and GJHZ20180928155207206). The authors also acknowledge the assistance of SUSTech Core Research Facilities.

REFERENCES

(1) Fattal, D.; Li, J. J.; Peng, Z.; Fiorentino, M.; Beausoleil, R. G. Flat Dielectric Grating Reflectors with Focusing Abilities. *Nat. Photonics* **2010**, *4*, 466−470.
(2) Rogers, E. T. F.; Lindberg, J.; Roy, T.; Savo, S.; Chad, J. E.; Dennis, M. R.; Zheludev, N. I. A Super-Oscillatory Lens Optical Microscope for Subwavelength Imaging. *Nat. Mater.* **2012**, *11*, 432−435.
(3) Yuan, G. H.; Zheludev, N. I. Detecting Nanometric Displacements with Optical Ruler Metrology. *Science* **2019**, *364*, 771−775.
(4) Kelzenberg, M. D.; Boettcher, S. W.; Petykiewicz, J. A.; Turner-Evans, D. B.; Putnam, M. C.; Warren, E. L.; Spurgeon, J. M.; Briggs, R. M.; Lewis, N. S.; Atwater, H. A. Enhanced Absorption and Carrier Collection in Si Wire Arrays for Photovoltaic Applications. *Nat. Mater.* **2010**, *9*, 239−244.
(5) Ali, M.; Zhou, F. L.; Chen, K.; Kotzur, C.; Xiao, C. L.; Bourgeois, L.; Zhang, X. Y.; MacFarlane, D. R. Nanostructured Photoelectrochemical Solar Cell for Nitrogen Reduction Using Plasmon-Enhanced Black Silicon. *Nat. Commun.* **2016**, *7*, 11335.
(6) Jeon, H. C.; Heo, C. J.; Lee, S. Y.; Yang, S. M. Hierarchically Ordered Arrays of Noncircular Silicon Nanowires Featured by Holographic Lithography Toward a High-Fidelity Sensing Platform. *Adv. Funct. Mater.* **2012**, *22*, 4268−4274.
(7) Wang, H. Y.; Jiang, X. X.; Lee, S. T.; He, Y. Silicon Nanohybrid-based Surface-enhanced Raman Scattering Sensors. *Small* **2014**, *10*, 4455−4468.
(8) Alhmoud, H.; Delalat, B.; Elnathan, R.; Cifuentes-Rius, A.; Chaix, A.; Rogers, M. L.; Durand, J. O.; Voelcker, N. H. Porous Silicon Nanodiscs for Targeted Drug Delivery. *Adv. Funct. Mater.* **2015**, *25*, 1137−1145.
(9) Tzur-Balter, A.; Shatsberg, Z.; Beckerman, M.; Segal, E.; Artzi, N. Mechanism of Erosion of Nanostructured Porous Silicon Drug Carriers in Neoplastic Tissues. *Nat. Commun.* **2015**, *6*, 6208.
(10) Lin, D. M.; Fan, P. Y.; Hasman, E.; Brongersma, M. L. Dielectric Gradient Metasurface Optical Elements. *Science* **2014**, *345*, 298−302.
(11) Arbabi, A.; Horie, Y.; Ball, A. J.; Bagheri, M.; Faraon, A. Subwavelength-Thick Lenses with High Numerical Apertures and Large Efficiency Based on High-Contrast Transmitarrays. *Nat. Commun.* **2015**, *6*, 7069.
(12) Proust, J.; Bedu, F.; Gallas, B.; Ozerov, I.; Bonod, N. All-Dielectric Colored Metasurfaces with Silicon Mie Resonators. *ACS Nano* **2016**, *10*, 7761−7767.
(13) Huang, K.; Dong, Z. G.; Mei, S. T.; Zhang, L.; Liu, Y. J.; Liu, H.; Zhu, H. B.; Teng, J. H.; Luk'yanchuk, B.; Yang, J. K. W.; Qiu, C. W. Silicon Multi-Meta-Holograms for the Broadband Visible Light. *Laser Photonics Rev.* **2016**, *10*, 500−509.
(14) Yang, Y. M.; Wang, W. Y.; Boulesbaa, A.; Kravchenko, I. I.; Briggs, D. P.; Puretzky, A.; Geohegan, D.; Valentine, J. Nonlinear Fano-Resonant Dielectric Metasurfaces. *Nano Lett.* **2015**, *15*, 7388−7393.
(15) Hulteen, J. C.; Vanduyne, R. P. Nanosphere Lithography - a Materials General Fabrication Process for Periodic Particle Array Surfaces. *J. Vac. Sci. Technol., A* **1995**, *13*, 1553−1558.
(16) Chen, K.; Rajeeva, B. B.; Wu, Z.; Rukavina, M.; Dao, T. D.; Ishii, S.; Aono, M.; Nagao, T.; Zheng, Y. Moiré Nanosphere Lithography. *ACS Nano* **2015**, *9*, 6031−6040.
(17) Hanarp, P.; Käll, M.; Sutherland, D. S. Optical Properties of Short Range Ordered Arrays of Nanometer Gold Disks Prepared by Colloidal Lithography. *J. Phys. Chem. B* **2003**, *107*, 5768−5772.
(18) Fredriksson, H.; Alaverdyan, Y.; Dmitriev, A.; Langhammer, C.; Sutherland, D. S.; Zäch, M.; Kasemo, B. Hole−Mask Colloidal Lithography. *Adv. Mater.* **2007**, *19*, 4297−4302.
(19) McLellan, J. M.; Geissler, M.; Xia, Y. N. Edge Spreading Lithography and Its Application to the Fabrication of Mesoscopic Gold and Silver Rings. *J. Am. Chem. Soc.* **2004**, *126*, 10830−10831.
(20) Liao, W. S.; Chen, X.; Chen, J.; Cremer, P. S. Templating Water Stains for Nanolithography. *Nano Lett.* **2007**, *7*, 2452−2458.
(21) Sun, Z. Q.; Li, Y.; Zhang, J. H.; Li, Y. F.; Zhao, Z. H.; Zhang, K.; Zhang, G.; Guo, J. R.; Yang, B. A Universal Approach to Fabricate Various Nanoring Arrays Based on a Colloidal-Crystal-Assisted-Lithography Strategy. *Adv. Funct. Mater.* **2008**, *18*, 4036−4042.
(22) Chen, J. X.; Liao, W. S.; Chen, X.; Yang, T. L.; Wark, S. E.; Son, D. H.; Batteas, J. D.; Cremer, P. S. Evaporation-Induced Assembly of Quantum Dots into Nanorings. *ACS Nano* **2009**, *3*, 173−180.
(23) Haynes, C. L.; Van Duyne, R. P. Nanosphere Lithography: A Versatile Nanofabrication Tool for Studies of Size-Dependent Nanoparticle Optics. *J. Phys. Chem. B* **2001**, *105*, 5599−5611.
(24) Lu, Y.; Yin, Y. D.; Xia, Y. N. Preparation and Characterization of Micrometer-Sized "Egg Shells". *Adv. Mater.* **2001**, *13*, 271−274.
(25) Xu, X.; Yang, Q.; Wattanatorn, N.; Zhao, C.; Chiang, N.; Jonas, S. J.; Weiss, P. S. Multiple-Patterning Nanosphere Lithography for Fabricating Periodic Three-Dimensional Hierarchical Nanostructures. *ACS Nano* **2017**, *11*, 10384−10391.
(26) Su, S.; Wu, Y.; Zhu, D.; Chao, J.; Liu, X. F.; Wan, Y.; Su, Y.; Zuo, X. L.; Fan, C. H.; Wang, L. H. On-Electrode Synthesis of Shape-Controlled Hierarchical Flower-Like Gold Nanostructures for Efficient Interfacial DNA Assembly and Sensitive Electrochemical Sensing of MicroRNA. *Small* **2016**, *12*, 3794−3801.
(27) Larsen, M. B.; Van Horn, J. D.; Wu, F.; Hillmyer, M. A. Intrinsically Hierarchical Nanoporous Polymers via Polymerization-Induced Microphase Separation. *Macromolecules* **2017**, *50*, 4363−4371.
(28) Kreder, M. J.; Alvarenga, J.; Kim, P.; Aizenberg, J. Design of Anti-Icing Surfaces: Smooth, Textured or Slippery? *Nat. Rev. Mater.* **2016**, *1*, 15003.
(29) Lv, T.; Cheng, Z.; Zhang, D.; Zhang, E.; Zhao, Q.; Liu, Y.; Jiang, L. Superhydrophobic Surface With Shape Memory Micro/Nanostructure and Its Application in Rewritable Chip for Droplet Storage. *ACS Nano* **2016**, *10*, 9379−9386.
(30) Liu, Y. J.; Cai, Z. Y.; Leong, E. S. P.; Zhao, X. S.; Teng, J. H. Optically Switchable Photonic Crystals Based on Inverse Opals Partially Infiltrated by Photoresponsive Liquid Crystals. *J. Mater. Chem.* **2012**, *22*, 7609−7613.
(31) Cai, Z. Y.; Liu, Y. J.; Teng, J. H.; Lu, X. M. Fabrication of Large Domain Crack-Free Colloidal Crystal Heterostructures with Superposition Bandgaps Using Hydrophobic Polystyrene Spheres. *ACS Appl. Mater. Interfaces* **2012**, *4*, 5562−5569.
(32) Cai, Z. Y.; Liu, Y. J.; Leong, E. S. P.; Teng, J. H.; Lu, X. M. Highly Ordered and Gap Controllable Two-Dimensional Non-Close-Packed Colloidal Crystals and Plasmonic-Photonic Crystals with Enhanced Optical Transmission. *J. Mater. Chem.* **2012**, *22*, 24668−24675.
(33) Cai, Z. Y.; Liu, Y. J.; Lu, X. M.; Teng, J. H. In Situ "Doping" Inverse Silica Opals with Size-Controllable Gold Nanoparticles for Refractive Index Sensing. *J. Phys. Chem. C* **2013**, *117*, 9440−9445.
(34) Cai, Z. Y.; Liu, Y. J.; Lu, X. M.; Teng, J. H. Fabrication of Well-Ordered Binary Colloidal Crystals with Extended Size Ratios for Broadband Reflectance. *ACS Appl. Mater. Interfaces* **2014**, *6*, 10265−10273.
(35) Zhang, Y.; Li, K.; Su, F. Y.; Cai, Z. Y.; Liu, J. X.; Wu, X. W.; He, H. L.; Yin, Z.; Wang, L. H.; Wang, B.; Tian, Y. Q.; Luo, D.; Sun, X. W.; Liu, Y. J. Electrically Switchable Photonic Crystals Based on Liquid-Crystal-Infiltrated TiO_2-Inverse Opals. *Opt. Express* **2019**, *27*, 15391−15398.
(36) Zhou, Z.; Li, Q.; Zhao, X. S. Evolution of Interparticle Capillary Forces during Drying of Colloidal Crystals. *Langmuir* **2006**, *22*, 3692−3697.
(37) Bakker, R. M.; Permyakov, D.; Yu, Y. F.; Markovich, D.; Paniagua-Domínguez, R.; Gonzaga, L.; Samusev, A.; Kivshar, Y.; Luk'yanchuk, B.; Kuznetsov, A. I. Magnetic and Electric Hotspots with Silicon Nanodimers. *Nano Lett.* **2015**, *15*, 2137−2142.

https://dx.doi.org/10.1021/acsami.9b22932
ACS Appl. Mater. Interfaces 2020, 12, 12345−12352

(38) Hu, L. T.; Liu, Y. J.; Han, Y. S.; Chen, P. X.; Zhang, C.; Li, C. H.; Lu, Z. Y.; Luo, D.; Jiang, S. Z. Graphene Oxide-Decorated Silver Dendrites for High-Performance Surface-Enhanced Raman Scattering Applications. *J. Mater. Chem. C* **2017**, *5*, 3908−3915.
(39) Zhang, C.; Li, C.; Yu, J.; Jiang, S.; Xu, S.; Yang, C.; Liu, Y. J.; Gao, X.; Liu, A.; Man, B. SERS Activated Platform with Three-Dimensional Hot Spots and Tunable Nanometer Gap. *Sens. Actuators, B* **2018**, *258*, 163−171.
(40) Lu, Z. Y.; Liu, Y. J.; Wang, M. H.; Zhang, C.; Li, Z.; Huo, Y. Y.; Li, Z.; Xu, S. C.; Man, B. Y.; Jiang, S. Z. A Novel Natural Surface-Enhanced Raman Spectroscopy (SERS) Substrate Based on Graphene Oxide-Ag Nanoparticles-Mytilus Coruscus Hybrid System. *Sens. Actuators, B* **2018**, *261*, 1−10.
(41) Wu, X. T.; Fan, X. K.; Yin, Z.; Liu, Y. J.; Zhao, J.; Quan, Z. W. Ordered Mesoporous Silver Superstructures with SERS Hot Spots. *Chem. Commun.* **2019**, *55*, 7982−7985.
(42) Schwartzberg, A. M.; Grant, C. D.; Wolcott, A.; Talley, C. E.; Huser, T. R.; Bogomolni, R.; Zhang, J. Z. Unique Gold Nanoparticle Aggregates as a Highly Active Surface-Enhanced Raman Scattering Substrate. *J. Phys. Chem. B* **2004**, *108*, 19191−19197.

https://dx.doi.org/10.1021/acsami.9b22932
ACS Appl. Mater. Interfaces 2020, 12, 12345−12352